SCIENTIFIC REPORTS

OPEN

Correspondence and requests for materials should be addressed to Z.W. (zcwang@wpi-aimr.tohoku.ac.jp) or S.H. (smhuang@phy.ecnu.edu.cn)

Atomic-Scale Observation of Migration and Coalescence of Au Nanoclusters on YSZ Surface by Aberration-Corrected STEM

Junjie Li[1,2], Zhongchang Wang[2], Chunlin Chen[2] & Sumei Huang[1]

[1]Engineering Research Center for Nanophotonics and Advanced Instrument, Ministry of Education, Department of Physics, East China Normal University, North Zhongshan Road 3663, Shanghai 200062, China, [2]Advanced Institute for Materials Research, Tohoku University, 2-1-1 Katahira, Aoba-ku, Sendai 980-8577, Japan.

Unraveling structural dynamics of noble metal nanoclusters on oxide supports is critical to understanding reaction process and origin of catalytic activity in heterogeneous catalysts. Here, we show that aberration-corrected scanning transmission electron microscopy can provide direct atomic-resolution imaging of surface migration, coalescence, and atomic rearrangement of Au clusters on an Y:ZrO$_2$ (YSZ) support. The high resolution enables us to reveal migration and coalescence process of Au clusters at the atomic scale, and to demonstrate that the coalesced clusters undergo a cooperative atomic rearrangement, which transforms the coherent into incoherent Au/YSZ interface. This approach can help to elucidate atomistic mechanism of catalytic activities and to develop novel catalysts with enhanced functionality.

Noble metal nanoclusters supported on oxides of high surface area are among the most important types of heterogeneous catalysts because of their unexpected chemical activity and high selectivity[1]. The catalytic performance of such heterogeneous systems depends on not only their chemical composition, but size and morphology of the nanoclusters and how the nanoclusters interact with oxide supports[2]. To date, a general consensus has been reached on several aspects of hybrid catalytic systems. The size of metal clusters remarkably influences catalytic properties, and nanoclusters often exhibit unusual physical and chemical behaviors which cannot be realized in their respective bulks[3–7]. In addition to the size effect, there is a strong support effect in which the oxide supports might tune catalytic properties by altering the shape and electronic nature of the metal clusters. Moreover, the active atoms and their oxidation states also take on practical significance in affecting catalytic properties. All these effects, including the preparation and processing behavior, rely on the migration, coalescence, and morphology transformation of the metal clusters due to their high surface energy arising from the reduced dimensions[2,8].

Several experimental techniques exist for investigating heterogeneous catalytic systems, yet, in general, no one can individually extract sufficient information of structure dynamics at the atomic level. X-ray scattering yields a spatially averaged structure and is thus insensitive to individual atoms[9]. Although scanning probe microscopy enables atoms to be identified, it falls short of probing the atoms far from surface[10]. Transmission electron microscopy (TEM) is, in principle, able to offer a direct observation of growth and mobility of Au clusters at the atomic scale[11–15]. However, for the conventional TEM, resolving spatially and identifying chemically metal clusters on oxide supports at dynamical condition still pose a non-trivial challenge.

Here, we apply aberration-corrected scanning TEM (STEM) to directly observe surface migration, coalescence, and atomic rearrangement of Au clusters on an Y:ZrO$_2$ (YSZ) (100) support at the atomic scale. The heterogeneous Au/YSZ system is chosen because it finds a plethora of applications as gas sensors[16,17], gas pumps[18], solid oxide fuel cells[19,20], and electrochemical reactors[21]. We offer definitive evidence that the Au/YSZ heterointerface can be initially epitaxial and coherent, and demonstrate that it undergoes structural rearrangement by migration and coalescence, which finally induces transformation of Au particles and also breaks coherency of the heterointerface.

Results

To avoid unwanted solvent effect, the heterogeneous catalytic system was prepared by depositing Au onto YSZ (100) TEM specimen using molecular beam epitaxy (MBE). Prior to the growth, TEM specimen was annealed at 973 K in air for 30 min to remove the amorphous layers. Figure 1a shows a representative high-angle annular-dark-field (HAADF) STEM image of the sample viewed from the YSZ [100] direction. Many clusters are located on the YSZ surface, which are identified as Au by the energy-dispersive x-ray spectroscopy (EDS) mapping (Supplementary Fig. S1). Moreover, the cross-section image reveals that surface of the YSZ support is atomically flat over extended regions up to several nanometers in size (Supplementary Fig. S2).

Since intensity of an atomic column in HAADF imaging mode is directly proportional to $\sim Z^{1.7}$ (Z: atomic number), image contrast is brighter for heavier atoms in the atomic column[22], which means that the brighter clusters represent Au, consistent with the EDS mapping. Figure 1b presents size distribution histogram of the Au clusters. The Au clusters vary in size from 0 to 3 nm with a mean value of $\sim$1.5 nm. Figure 1d shows an enlarged HAADF STEM image viewed from the YSZ [100] direction. Two types of spots with different image contrast are detected: the lighter ones represent pure Zr atomic columns (Fig. 1c), while the randomly distributed brighter ones represent Zr atomic columns containing a single Au atom (marked with arrows). The difference in image contrast can also be corroborated in the image intensity profile obtained across a single Au atom (Fig. 1d,

inset). As a confirmation, we simulated the HAADF STEM image using a model comprising of a single Au atom on top of an YSZ slab, and compared the simulated image and image intensity profile (Supplementary Fig. S3) with their experimental counterparts (Fig. 1d). We find a good agreement, offering further support to the presence of a single Au atom on top of Zr atomic columns. It is worthy of noting that the presence of Y atoms alone cannot give rise to the variation in image contrast because they are evenly distributed in the YSZ and also for their very close atomic number to that of Zr.

Figure 2 shows atomic-resolution HAADF and bright-field (BF) STEM image of the Au nanoclusters in different size. The corresponding STEM image intensity profiles uncover that the Au nanoclusters are thin with a few atomic layers (Supplementary Fig. S4), as confirmed in the cross-sectional image (Supplementary Fig. S2), which also reveals a trapezoidal shape for the Au clusters. All the Au atoms in the clusters prefer residing on top of Zr atoms, as seen in the case of single Au atoms (Fig. 1d). In addition, the Au atoms assemble to form a face-centered cubic (FCC) structure, and the interface is epitaxial and coherent, irrespective of dimension of the nanoclusters. The interface coherency is also reflected in the BF STEM images in which dark spots denote atomic columns, and in the cross-sectional STEM image (Supplementary Fig. S2).

To shed light on dynamics of the Au nanoclusters, we show sequential atomic-resolution HAADF STEM images in Fig. 3. The nanoclusters are stable before electron beam irradiation owing to their interaction with the substrate, yet are prone to migrate under
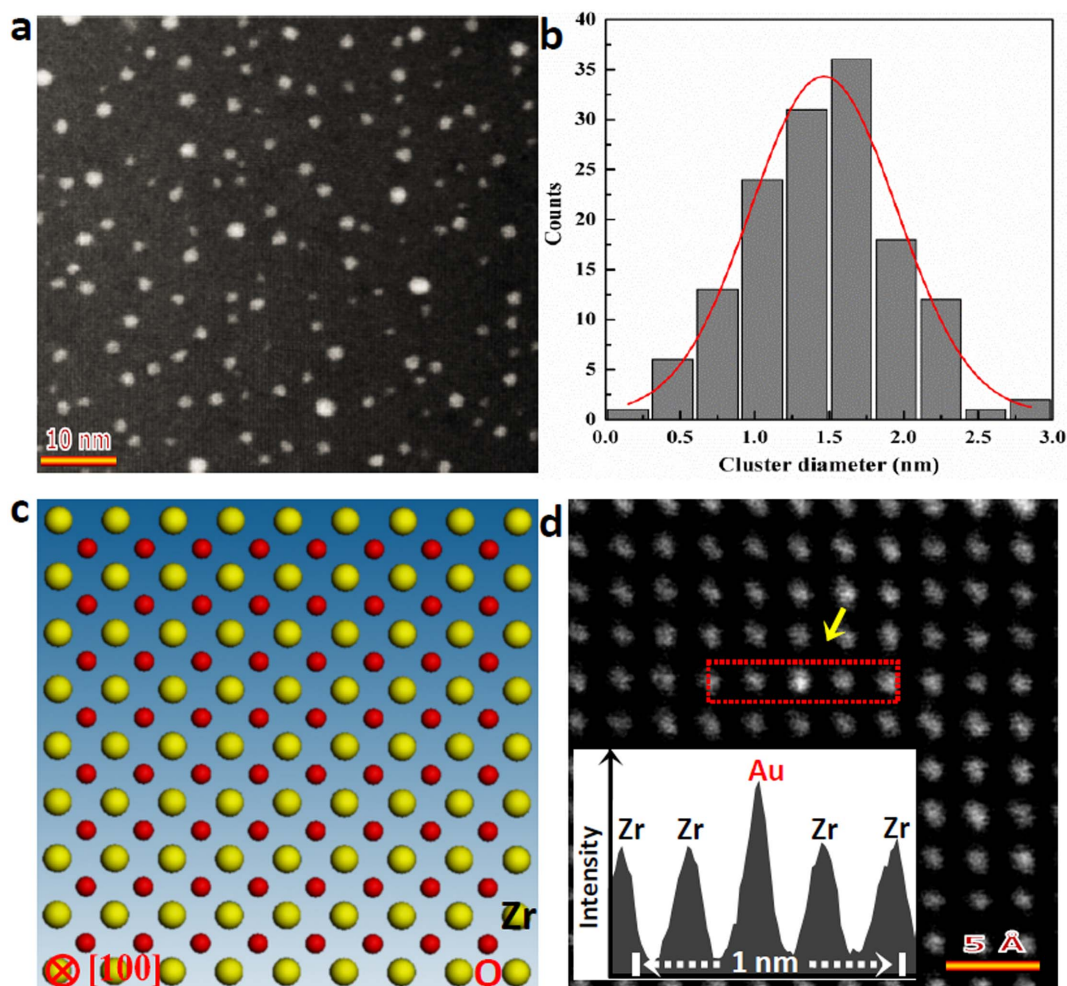
Figure 1 | Morphology, size distribution, and structure of the Au/YSZ system. (a), A typical HAADF STEM image of Au clusters on YSZ (100) surface. (b), Histogram showing the size distribution of Au clusters. (c), Atomic model of bulk YSZ viewed from [100] direction. (d), Atomic-resolution HAADF STEM image of individual Au atom viewed from [100] direction. Inset shows image intensity profile across a single Au atom.
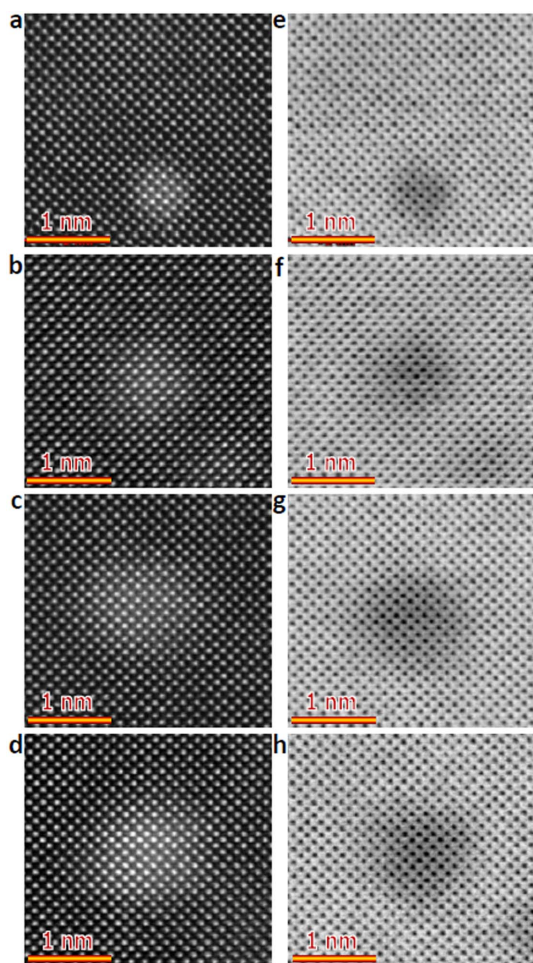
Figure 2 | Plan-view imaging of Au clusters in different size. HAADF (a–d) and BF (e–h) STEM images of the Au clusters on the YSZ substrate viewed from [100] direction.

the electron beam. On inspection of two close nanoclusters (labeled 1 and 2), we find that coalescence occurs by shortening the distance between the clusters from ~0.8 to ~0.56 nm after 150 s, and then to ~0.35 nm after 270 s (Fig. 3g–i). The two nanoclusters are eventually connected through a narrow neck. Interestingly, the epitaxy and coherency between the cluster and the support are maintained during the entire migration process, albeit that the shape of the clusters is altered during migration.

Figure 4 shows a coalescence process of the two Au clusters as a function of irradiation time. Interestingly, the two Au clusters are merged directly at the atomic scale, which can be attributed to the epitaxy between the clusters and YSZ. Such behavior is in striking contrast to the unification of Au nanocrystals, which is assisted by crystal rotation or grain boundary migration[23,24]. Moreover, the whole coalescence process is completed rapidly in 210 s (Fig. 4), as opposed to the coalescence of Au nanoclusters which takes longer time because grain boundary often slows down interdiffusion. The Au atoms in merged clusters finally undergo a substantial rearrangement after coalescence, transforming the clusters to ball shape (Fig. 4i).

Discussion

The migration and coalescence of Au clusters and associated structural rearrangement and shape change can in principle be attributed to knock-on momentum transfer and thermal effect arising from electron beam[25–27]. The transferred kinetic energy depends on not only the ratio of electron to nuclei mass but the acceleration voltage

of STEM. The transferred energy reaches maximum once the head-on collisions occur. Since an acceleration voltage of 300 kV is adopted, atom displacement in bulk Au is not expected to take place. However, the bonds in Au clusters may break and thus displace individual Au atoms during STEM observation[28], which eventually results in migration of the nanoclusters.

When two nanoclusters come to contact, the bonding rearrangement may result in local increase in temperature (*e.g.* over 100 K for a cluster of 500 atoms[29]), which can accelerate the coalescence process *via* enhancing surface migration. This may provide an explanation to the observation that shape of the Au clusters reaches equilibrium in a short time during the coalescence process.

After the coalescence, the Au nanoclusters undergo a cooperative atomic rearrangement in order to minimize their total energy. Based on the macroscopic concept and strain effect, total energy (E_{tot}) of the clusters can be expressed as:

$$E_{tot} = \mu_v N_v + \mu_e N_e + \mu_i N_i + \mu_s N_s + \mu_b N_b + E_{strain}, \quad (1)$$
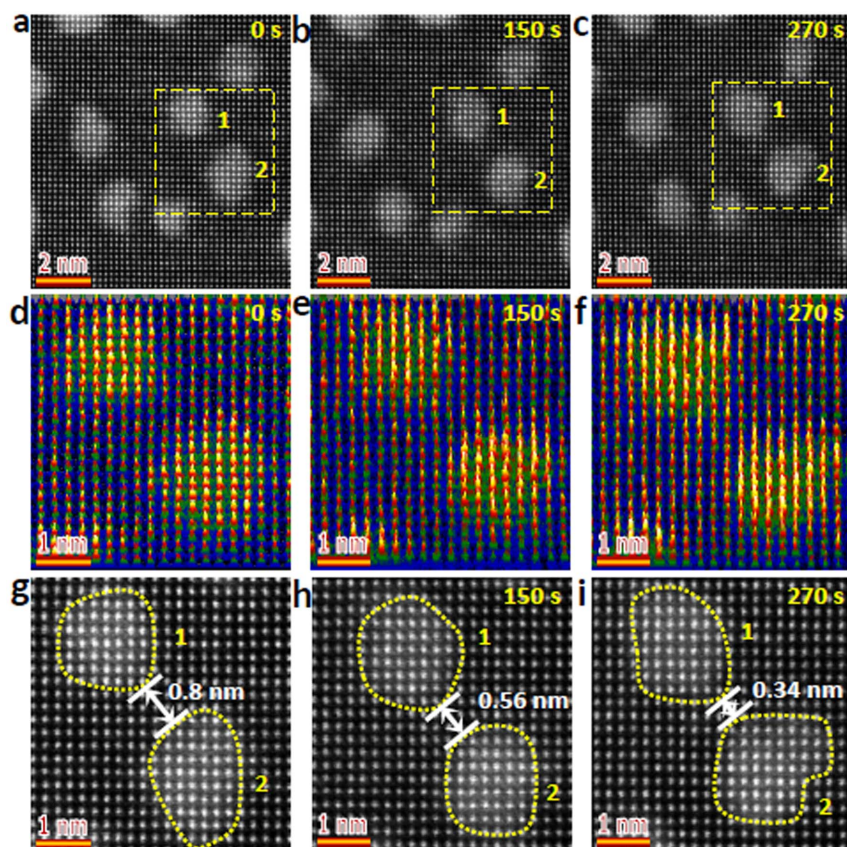
where μ_α represents specific energy per atom for the atoms at the vertex ($\alpha = v$), on the edge ($\alpha = e$), at the interface ($\alpha = i$), on the surface ($\alpha = s$), and in the bulk ($\alpha = b$); N_α is the number of atoms; and E_{strain} is strain energy. According to this formulae, the clusters less than 3 nm are calculated to favor either an icosahedral or decahedral configuration, while those larger than 3 nm prefer a truncated octahedron configuration[29,30].

To test this prediction, we show in Fig. 5 an entire process of migration, coalescence, and cooperative atomic rearrangement of Au clusters. In Fig. 5a–e, a large cluster forms via migration and coalescence of three relatively smaller ones. To minimize total surface stress, ratio of surface to volume, and surface energy, the large cluster subsequently undergoes a substantial shape alternation by surface migration and atomic rearrangement (Fig. 5e–i). The Au cluster is eventually transformed to a truncated octahedron after ~4 min, consistent with the above calculation result[30]. Moreover, we find interestingly that there appear moiré fringes in the images taken at the final stage of atomic rearrangement, suggesting that the Au/YSZ heterointerface turns incoherent. This offers definitive evidence that shape transformation of the large Au clusters is accompanied with a structural transition at the interface.

To conclude, we show that aberration-corrected STEM can be used to extract real-time information on migration, coalescence, and atomic rearrangement of heterogeneous catalytic systems at the atomic scale. The direct observation of oxide-supported Au clusters has crucial implications for understanding diffusion dynamics, coalescence process, and functionality of clusters in catalysts. Such atomic-scale technique allows us to demonstrate that the coalesced clusters undergo atomic rearrangement, forming a stable facet structure. The observed shape evolution of the large Au clusters is accompanied by structural transformation from coherent to incoherent Au/YSZ interface. Such experimental ability to unravel migration, coalescence, and atomic rearrangement of oxide-supported metal cluster helps to elucidate atomistic origin of catalytic activities in many heterogeneous catalytic systems.

Methods

Figure 3 | Spatial evolution of Au clusters with irradiation time. (a–c), Sequential HAADF STEM images viewed from [100] projection showing migration of Au clusters on YSZ. (d–f), Intensity surface plots. (g–i), Enlarged HAADF STEM images. The outline of the two clusters is marked by a dotted curve.
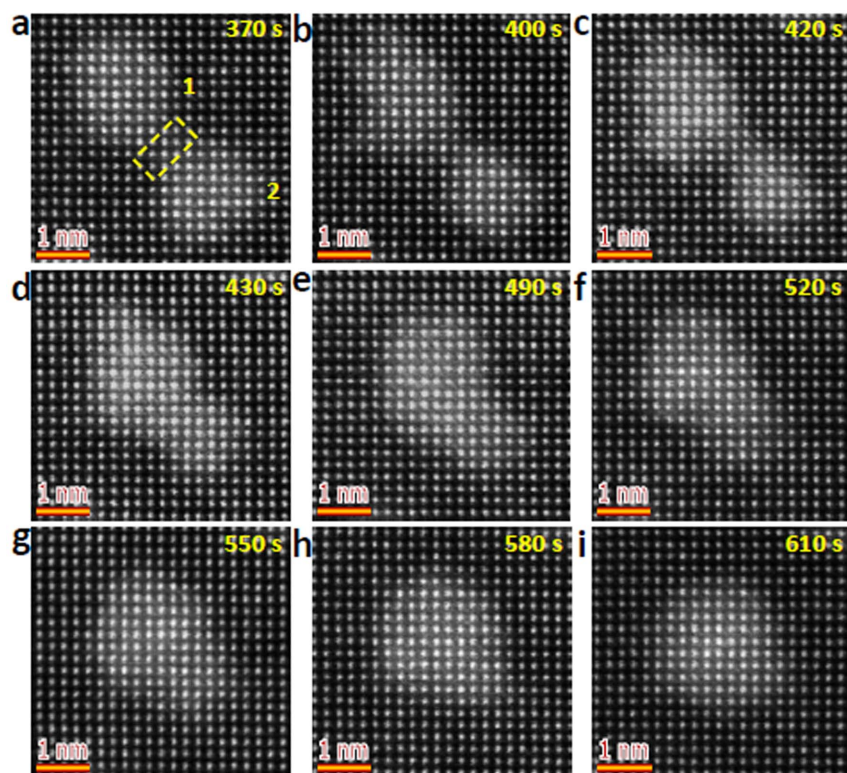
Figure 4 | Direct imaging of the coalescence process. (a–i) HAADF STEM images viewed from [100] direction showing evolution of the two nanoclusters as a function of time. The open square in (a) indicates the neck area in between two nanoclusters at the initial stage of the coalescence. The total dose of electron beam is 4301.2 e/nm^2.
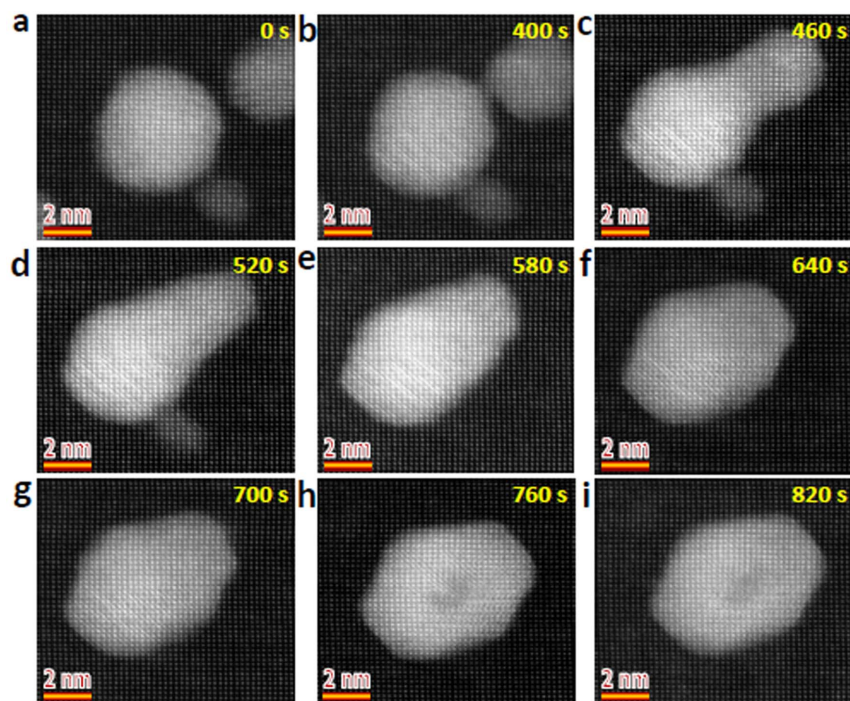
Figure 5 | Migration and coalescence of large Au clusters. HAADF STEM images showing migration and coalescence process at the atomic scale (a–e), and atomic rearrangement of the merged clusters (e–i). The merged clusters are eventually transformed to truncated octahedra. The total dose of electron beam is 5782.0 e/nm².

the YSZ substrates directly, followed by cutting, grinding, dimpling and Ar ion-beam thinning.

STEM imaging. HAADF and BF STEM images were taken using double aberration-corrected Titan Cubed G2 60–300 analytical microscope which was equipped with an X-FEG Schottky high brightness source and a monochromator. The microscope was operated at 300 kV. The spatial resolution of the STEM is ~0.7 nm, which provides an unprecedented opportunity to probe structures with sub-Ångström resolution. Images were recorded on a charge-coupled device (CCD) camera (2k × 2k, Gatan UltraScan 1000). For the HAADF STEM imaging, a probe convergence angle of ~22 mrad and a detector with an inner semiangle of over 60 mrad were adopted. The EDS was used to analyze chemical composition. The electron density used in observation was estimated to be 7.1 e/nm²s⁻¹. The HAADF STEM image simulation was performed using a model comprising a single Au atom on top of Zr atomic column using the WinHREM program (HREM Research Inc.), which was based upon the multislice method.

1. Qiao, B. *et al.* Single-atom catalysis of CO oxidation using Pt₁/FeOₓ. *Nat. Chem.* **3**, 634–641 (2011).
2. Lu, J., Elam, J. W. & Stair, P. C. Synthesis and stabilization of supported metal catalysts by atomic layer deposition. *Accounts Chem. Res.* **46**, 1806–1815 (2013).
3. Scholl, J. A., Koh, A. L. & Dionne, J. A. Quantum plasmon resonances of individual metallic nanoparticles. *Nature* **483**, 421–428 (2012).
4. Bingham, J. M., Anker, J. N., Kreno, L. E. & Van Duyne, R. P. Gas sensing with high-resolution localized surface plasmon resonance spectroscopy. *J. Am. Chem. Soc.* **132**, 17358–17359 (2010).
5. Awazu, K. *et al.* Plasmonic Photocatalyst Consisting of Silver Nanoparticles Embedded in Titanium Dioxide. *J. Am. Chem. Soc.* **130**, 1676–1680 (2008).
6. Tian, Y. & Tatsuma, T. Mechanisms and applications of plasmon-induced charge separation at TiO2 films loaded with gold nanoparticles. *J. Am. Chem. Soc.* **127**, 7632–7637 (2005).
7. Liu, Z., Hou, W., Pavaskar, P., Aykol, M. & Cronin, S. B. Plasmon Resonant Enhancement of Photocatalytic Water Splitting Under Visible Illumination. *Nano Lett.* **11**, 1111–1116 (2011).
8. Asoro, M. A., kovar, D., Shao-Horn, Y., Allard, L. F. & Ferreira, P. J. Coalescence and sintering of Pt nanoparticles: *in situ* observation by aberration-corrected HAADF STEM. *Nanotechnology* **21**, 025701–025706 (2010).
9. Ehrlich, G. Direct observations of the surface diffusion of atoms and clusters. *Surf. Sci.* **246**, 1–12 (1991).
10. Moram, M. A., Oliver, R. A., Kappers, M. J. & Humphreys, C. J. The spatial distribution of threading dislocations in gallium nitride films. *Adv. Mater.* **21**, 3941–3944 (2009).
11. Wang, Z. C. *et al.* Atom-resolved imaging of ordered defect superstructures at individual grain boundaries. *Nature* **479**, 380–383 (2011).
12. Wang, Z. W. & Palmer, R. E. Direct atomic imaging and dynamical fluctuations of the tetrahedral Au20 Cluster. *Nanoscale* **4**, 4947–4949 (2012).
13. Zan, R., Bangert, U., Ramasse, Q. & Novoselov, K. S. Evolution of Gold Nanostructures on Graphene. *Small* **7**, 2868–2872 (2011).
14. Métois, J. J., Heinemann, K. & Poppa, H. *In situ* investigation of the mobility of small gold clusters on cleaved MgO surfaces. *Appl. Phys. Lett.* **29**, 134–136 (1976).
15. Schwartzkopf, M. *et al.* From atoms to layers: *in situ* gold cluster growth kinetic during sputter deposition. *Nanoscale* **5**, 5053–5062 (2013).
16. Mori, M. *et al.* Detection of offensive odorant in air with a planar-type potentiometric gas sensor based on YSZ with Au and Pt electrodes. *Sensor Actuators B* **191**, 351–355 (2014).
17. Schonauer-Kamin, D., Fleischer, M. & Moos, R. Half-Cell Potential Analysis of an Ammonia Sensor With The Electrochemical Cell Au|YSZ|Au, V₂O₅-WO₃-TiO₂. *Sensors* **13**, 4760–4780 (2013).
18. Ciacchi, F. T., Badwal, S. P. S. & Zelizko, V. Tubular zirconia-yttria electrolyte membrane technology for oxygen separation. *Solid State Ionics* **763**, 152–153 (2002).
19. Raźniak, A., Dudek, M. & Tomczyk, P. Reduction of oxygen at the interface M|solid oxide electrolyte (M = Pt, Ag and Au, solid oxide electrolyte = YSZ and GDC). Autocatalysis or artifact? *Catal. Today* **176**, 41–47 (2011).
20. Ruggiero-Mikoajczyk, Suskib, M. L., Mordarski, G., Koacz, J. & Grabowski, R. Dependencies of the open-circuit voltage of Au/YSZ/Pt single-chamber fuel on the composition of the uniform CH₄+O₂ gas mixture with the solid carbon deposition. *Electrochim. Acta* **55**, 8513–8516 (2010).
21. Chen, M. S. & Goodman, D. W. Structure-activity relationships in supported Au catalysts. *Catal. Today* **116**, 111–120 (2006).
22. Pennycook, S. J. & Jesson, D. E. High-Resolution Z-Contrast Imaging of Crystals. *Ultramicroscopy* **37**, 14 (1991).
23. Yuk, J. M. *et al.* *In situ* atomic imaging of coalescence of Au nanoparticles on grapheme: rotation and grain boundary migration. *Chem. Commun.* **49**, 11479–11481 (2013).
24. Zan, R., Bangert, U., Ramasse, Q. & Novoselov, K. S. Evolution of Gold Nanostructures on Graphene. *Small* **7**, 2868–2872 (2011).
25. Hobbs, L. W. *Introduction to analytical Electron Microscopy* (Plenum, New York, 1979).
26. Zheng, H. *et al.* Observation of Single Colloidal Platinum Nanocrystal Growth Trajectories. *Science* **324**, 1309–1312 (2009).
27. Zaluzec, N. J. & Mansfield, J. F. *Intermediate Voltage Microscopy and Its Application to Materials Science* (Philips Electron Optics Publishing Group, New Jersey, 1987).
28. Williams, D. B. & Cater, C. B. *In Transmission Electron Microscopy* (Plenum, New York, 1996).
29. Baletto, F. & Ferrando, R. Structural properties of nanoclusters: Energetic, thermodynamic, and kinetic effects. *Rev. Modern Phys.* **77**, 371–423 (2005).

30. Barnard, A. S., Lin, X. M. & Curtiss, L. A. Equilibrium Morphology of Face-Centered Cubic Gold Nanoparticles > 3 nm and the Shape Changes Induced by Temperature. *J. Phys. Chem. B* **109**, 24465–24472 (2005).

Acknowledgments

Author contributions

J.J.L. prepared the samples, took the images, and wrote the paper. C.C. took the images. S.H. discussed the results. Z.W. wrote the paper and directed the entire study. All authors read and commented on the paper.

Additional information